The Thores Lake proglacial system: remnant stability in the rapidly changing Canadian High Arctic

Alexander I. Culley [a,b,c], Mary Thaler[a,b,c], William Kochtitzky [d], Pilipoosie Iqaluk[e], Josephine Z. Rapp [a,b,c], Milla Rautio[f], Michio Kumagai[g], Luke Copland[d], Warwick F. Vincent [b,c,h], and Catherine Girard [b,c,f]

[a]Département de biochimie, de microbiologie et de bio-informatique, Université Laval, Québec, QC, Canada; [b]Institut de biologie intégrative et des systèmes (IBIS), Université Laval, Québec, QC, Canada; [c]Centre d'études nordiques (CEN), Université Laval, Québec, QC, Canada; [d]Department of Geography, Environment and Geomatics, University of Ottawa, Ottawa, ON, Canada; [e]Hunters and Trappers Association, Resolute Bay, NU, Canada; [f]Département des sciences fondamentales, Université de Québec à Chicoutimi, Chicoutimi, QC, Canada; [g]Lake Biwa and Sigma Research Center, Ritsumeikan University, Kusatsu, Japan; [h]Département de biologie, Université Laval, Québec, QC, Canada

Corresponding author: **Dr. Catherine Girard** (email: catherine5_girard@uqac.ca)

Abstract

We describe limnological data sets from Thores Lake, a large ice-contact proglacial lake in northern Ellesmere Island, Nunavut (82.65°N), including longitudinal and cross transects (vertical resolution 0.03 m, horizontal resolution 100–200 m). The lake is formed due to damming by Thores Glacier at its northwest margin, has multi-year ice cover and a cold (<1.54 °C) fresh water column with a bottom layer of <0 °C, high-conductivity water in the deepest basin. Thores Lake is ultraoligotrophic, with low nutrient and phytoplankton stocks. Accessory pigment data and metagenomics were used to describe the eukaryotic microbial community. Diversity and taxonomic composition in the water column were homogeneous down to a depth of 40 m, consistent with density profiles. Surface water at the glacier interface was characterized by high turbidity and total phosphorus concentrations, and a distinct phytoplankton community dominated by chlorophytes, whereas the lake water column had higher relative abundances of chrysophytes and photosynthetic dinoflagellates. Thores Lake has a contracted pelagic food web, with the highest trophic level occupied by phytoplankton-feeding rotifers, and no crustacean zooplankton; profiles showed that omega-3 fatty acids (FAs) ranged from <1% (glacier interface) to 3.6% (central lake) of total seston FAs. Given the stability of the Thores Glacier ice dam and the persistence of cold water capped by perennial ice, Thores Lake provides a baseline to assess the impact of climate change on far northern lakes.

Key words: proglacial lake, ultraoligotrophic, Arctic, microbial eukaryotes, zooplankton

Introduction

Lakes in the High Arctic can be viewed as sentinels of regional and global climate change (Mueller et al. 2009). On the northern coast of Ellesmere Island, Nunavut, Canada, lakes are distinguished by multi-year ice cover and microbial-dominated food webs (Vincent et al. 2011), but warming has caused abrupt regime shifts in their ice cover, affecting underwater light and water column mixing (Mueller et al. 2009; Bégin et al. 2021a). This steep, mountainous region is glacierized over much of its surface, particularly at high elevation, and experiences a cooling effect from thick sea ice and marginal ice shelves to the north (Vincent and Mueller 2020). Regional trends have shown increasing air and ocean temperatures since at least 1990 (White and Copland 2019; Bégin et al. 2021a), but little is known about the impacts on proglacial lakes.

Large-scale standardized limnological data sets (e.g., Filazzola et al. 2020) are increasingly recognized as important for evaluating the impact of human activities on ecosystem health, and Arctic-specific databases have compiled lake morphology and (or) water chemistry for thousands to millions of lakes (e.g., Dranga et al. 2018; Stolpmann et al. 2021; Sui et al. 2022). However, it is rare to find depth-distributed data in such compilations. The northern environmental data archive Nordicana (series D), where this data set is archived, provides detailed profiling and time series (e.g., NEIGE 2017) data for many lakes in northern Canada, as well as compiled data for shallow waters across the circumpolar North (Wauthy et al. 2017).

This article describes the first limnological data and other environmental observations from Thores Lake, a proglacial lake in northern Ellesmere Island. The lake is dammed by the Thores Glacier that, unlike many glacial features in this region, appears to have been fairly stable in its extent over the past few decades (Kochtitzky et al. 2022). The data sets include physico-chemical profiles along transects, observations of microbial plankton by pigment and molecular analysis, and evaluation of zooplankton community and fatty acid (FA)

Fig. 1. (A) Regional map and watershed of Thores Lake. The watershed contains eight glaciers, of which the largest is Thores Glacier. Unglacierized areas appear grey-brown in this image. Image from Sentinel-2 satellite, 27 July 2021. (B) Aerial view of glacier terminus into lake (photo by William Kochtitzky). Blue arrow shows glacier interface sampling site. (C) Sampling locations on Thores Lake. Water column samples were collected through the lake ice. Black arrow shows water column sampling location in 2018. Zooplankton sampling sites are marked with a "Z". Nutrients, turbidity, and fatty acid water column sampling sites are marked with an "N". Photosynthetically active radiation sites are marked with a "P". White arrows show input streams into the lake. Satellite image from 3 August 2021, accessed from Planet Labs under the Education and Research Program license (Planet Team 2017).
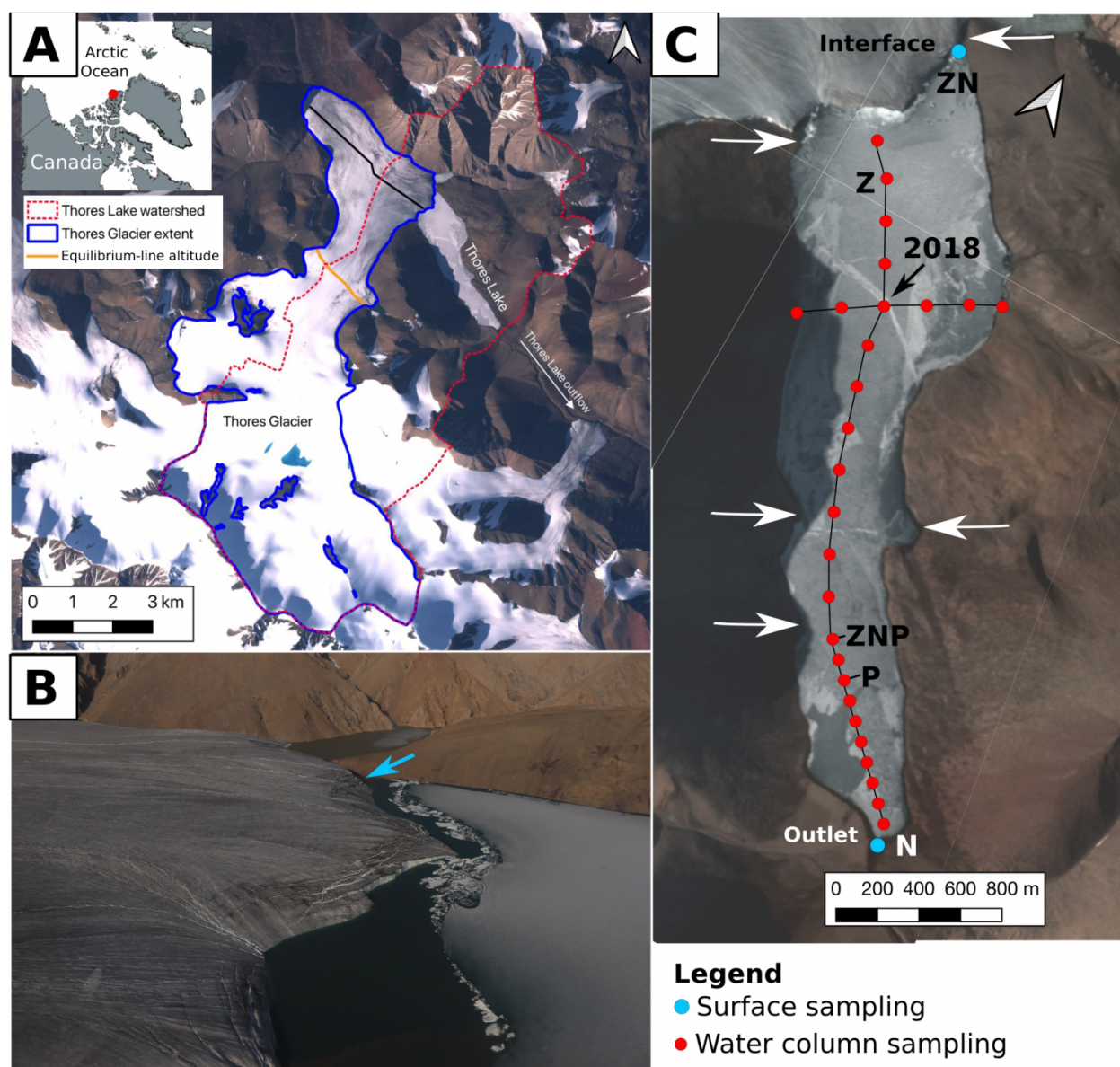
composition. These data were collected as part of the Terrestrial Multidisciplinary Distributed Observatories for the Study of the Arctic Connections project (T-MOSAiC; Vincent et al. 2019), with the aim of providing a baseline data set for assessing ongoing change in the fast-warming High Arctic.

Materials and methods

Study site

Thores Glacier and Thores Lake (82.65°N; 73.68°W) are located 44 km inland from the Arctic Ocean, and 400 m above

sea level. Thores River leaves the lake to the southeast, flowing into Disraeli Fiord in the vicinity of the Disraeli Glacier terminus. Satellite imagery shows that Thores Glacier covers an area of 43 km^2 (Fig. 1A). It has experienced relatively little change in extent since at least the Little Ice Age (Kochtitzky et al. 2022).

Thores Lake has a surface area of 2.16 km^2, being 3.7 km long, and 1 km across at its widest point at the glacier terminus end (Fig. 1C). The catchment area is 64.2 km^2, of which Thores Glacier makes up 46% (29.8 km^2) (Fig. 1A). Seven other glaciers, all but one <0.25 km^2 in area, make up a combined 12% of the watershed, while the remainder (including the

area of Thores Lake) is unglacierized. Vegetation in this polar desert catchment is sparse, consisting of small ground plants where present (details in Vincent et al. 2011).

Lake depth was measured using an RBRconcerto³ CTD++ logger (RBR Ltd., Ottawa, ON, Canada). The lake basin deepens along the longitudinal transect from 4 m near the outflow to a maximum recorded depth of 69 m located ~240 m from the glacier terminus (Fig. 2). We therefore identify a deep northern basin near the glacier, and a shallower southern basin, though there is no distinct sill separating them. Limited bathymetry data prevent us from calculating the total lake volume, but using an approximate average depth of 34 m and an annual water equivalent snowfall of 0.15 m year^{-1} over the Thores Lake watershed (as measured at the Alert weather station, 160 km west of Thores Lake; Bégin et al. 2021a), we estimate a residence time between 7 and 15 years depending on loss to evaporation. Discharge of Thores River immediately downstream of the lake was estimated on 21 July 2019 by ice float velocities (0.6–1.4 m s^{-1}) and trapezoidal integration over eight depth-measured segments; this gave a value of 7.6 m³ s^{-1}, equivalent to approximately 1% of the lake volume per day.

We manually inspected optical satellite imagery to see whether Thores Lake has recently completely lost its ice cover, using ASTER (2000 to present), Landsats 4, 5, 7, 8, and 9 (1999 to present), and Planet Labs including RapidEye and Skysat (2009 to present). While nearly all years showed at least some open water, no image shows a completely ice-free Thores Lake (Supplementary Video S1). However, given the limited data availability in the region, we cannot rule out that Thores Lake has been ice-free at some point prior to 1999.

Although Thores Lake remains ice covered year-round, in most summers it develops a marginal moat, such that the ice is not attached to the shore or glacier terminus (Supplementary Video S1). Moat width in July 2019 varied according to wind conditions, between 1 and >10 m. The middle part of the lake is traversed by leads that re-occur every year (Supplementary Video S1), and appeared to correspond to input streams entering the lake. We observed a turbid plume from a stream, originating on Thores Glacier, which enters the northwest side of the lake (Fig. 1C) after flowing alongside the glacier for ~1400 m. A similar, but shorter stream enters the lake on the northeast side.

Sample collection and processing

On 28 July 2018, we collected triplicate surface water samples (<0.5 m) from the lake outlet and in contact with the glacier (hereafter "glacier interface"), and sampled the water column in the middle of the lake (Fig. 1C) from three holes bored in the ice cover within 10 m of each other. Water column properties, including conductivity, temperature, and chlorophyll a (chl a) fluorescence, were measured from a single hole using the RBR logger with a frequency of 6 measurement s^{-1}, which yielded a vertical resolution of ~0.03 m. The manufacturer's stated accuracy for this instrument is ±0.003 mS cm^{-1}, ± 0.002 °C, ±0.05 m, and ± 8 µmol/L oxygen, with a detection limit of 0.025 µg L^{-1} for chl a. To process RBR data, we used the downcast only and removed values taken in air

(negative depth). Measurements where the RBR logger hit the bottom sediments, evidenced by a spike of conductivity values, were removed manually. Specific conductivity and temperature were converted to water density following Millero et al. (1980); we could not correct for the effects of specific ionic ratios as in Bégin et al. (2021b), since these are not presently known. Dissolved oxygen (DO) concentration was measured every 1–5 m with an EXO2 sonde (YSI, Yellow Springs, OH, USA). Water samples were collected for pigments and DNA using a 7 L Limnos sampler (Limnos.pl, Komorów, Poland) at 5, 17, and 40 m depths, as well as from the surface water at the outlet of the lake, the glacier interface, and from a melted core of lake ice (pigments only) that was thawed over 36 h in the dark at 4 °C. Containers for collection were cleaned with 2% (v/v) Contrad™70 detergent (Decon Laboratories, King of Prussia, PA) and 10% HCl (ACS grade, Sigma–Aldrich, Oakville, ON, Canada), and filtered within 8 h of collection. Pigment samples were analyzed upon returning to the laboratory using high-performance liquid chromatography (HPLC), as in Thaler et al. (2017). Based on the water volumes filtered, the detection limit for chlorophyll pigments (quantified by fluorometry in the HPLC) was around 0.05 µg L^{-1} and the detection limit for the carotenoid accessory pigments (quantified by absorbance in the 5 mm photodiode array detector) was around 0.1 µg L^{-1}. For microbial analyses, triplicate samples (from each sampling hole) of 340–600 mL (Supplementary Table S1) were filtered onto 0.02 µm pore size Whatman™ Anotop™ filters (Marlborough, USA), without pre-filtration. Filters were immediately frozen at −20 °C in the field and then stored at −80 °C until extraction.

During 17–23 July 2019, the same water column properties were measured as in 2018, with the difference that DO was measured with the RBR logger. Measurements were taken along a longitudinal transect of 22 holes drilled into the lake ice 100–200 m apart, as well as a cross transect of 5 additional holes ~0.82 km from the glacier terminus (Fig. 1C). The transects crossed each other at the 2018 sampling site. Surface water was also sampled at the glacier interface and lake outlet. Physico-chemical data in 2019 were visualized using Ocean Data View v.4.7.4 (Schlitzer 2015), and are summarized in Table 1. Photosynthetically active radiation (PAR) was measured at two sites in the southern basin (Fig. 1C) by lowering a LI-192 sensor (LI-COR Biosciences, Lincoln, NE) to 9 m below the ice.

Water chemistry samples, including total phosphorus (TP), total nitrogen (TN), nitrite and nitrate nitrogen (NO$_3$), and dissolved organic carbon (DOC), were collected at 5 and 15 m depth (Fig. 1C), as well as from the surface at the lake outlet and glacier interface. Water samples, 40 mL for TP and TN and 80 mL for NO$_3$ and DOC, were preserved with 5 mmol/L H$_2$SO$_4$. TP, TN, and DOC samples were analyzed at l'Université du Québec à Montréal (UQAM, Montréal) following established protocols (Cuthbert and del Giorgio 1992; Wetzel and Likens 2000; Patton and Kryskalla 2003). The limits of detection for these analyses were 0.008 mg TN L^{-1}, 0.5 µg TP L^{-1}, 0.01 mg NO$_3$-N L^{-1}, and 0.05 mg DOC L^{-1}.

Samples for FAs in seston were collected using the Limnos sampler at 5 and 15 m depths at the same site as nutrients, and directly into Nalgene bottles from surface water at

Fig. 2. Water column properties of Thores Lake in 2019 in longitudinal (left) and cross (right) section (as shown in Fig. 1C). Dashed line shows 2018 sampling location, which is also the intersection with the cross transect. Locations of open water leads are marked with arrows in the top panel (A). Euphotic depth (irradiance is 1% incident values above the ice) identified by an asterisk in (D) at the two sites where it was measured. Dissolved oxygen values are unavailable for two sites near the outlet and in the southern basin. Data were visualized with Ocean Data View v. 4.7.4 (Schlitzer 2015).
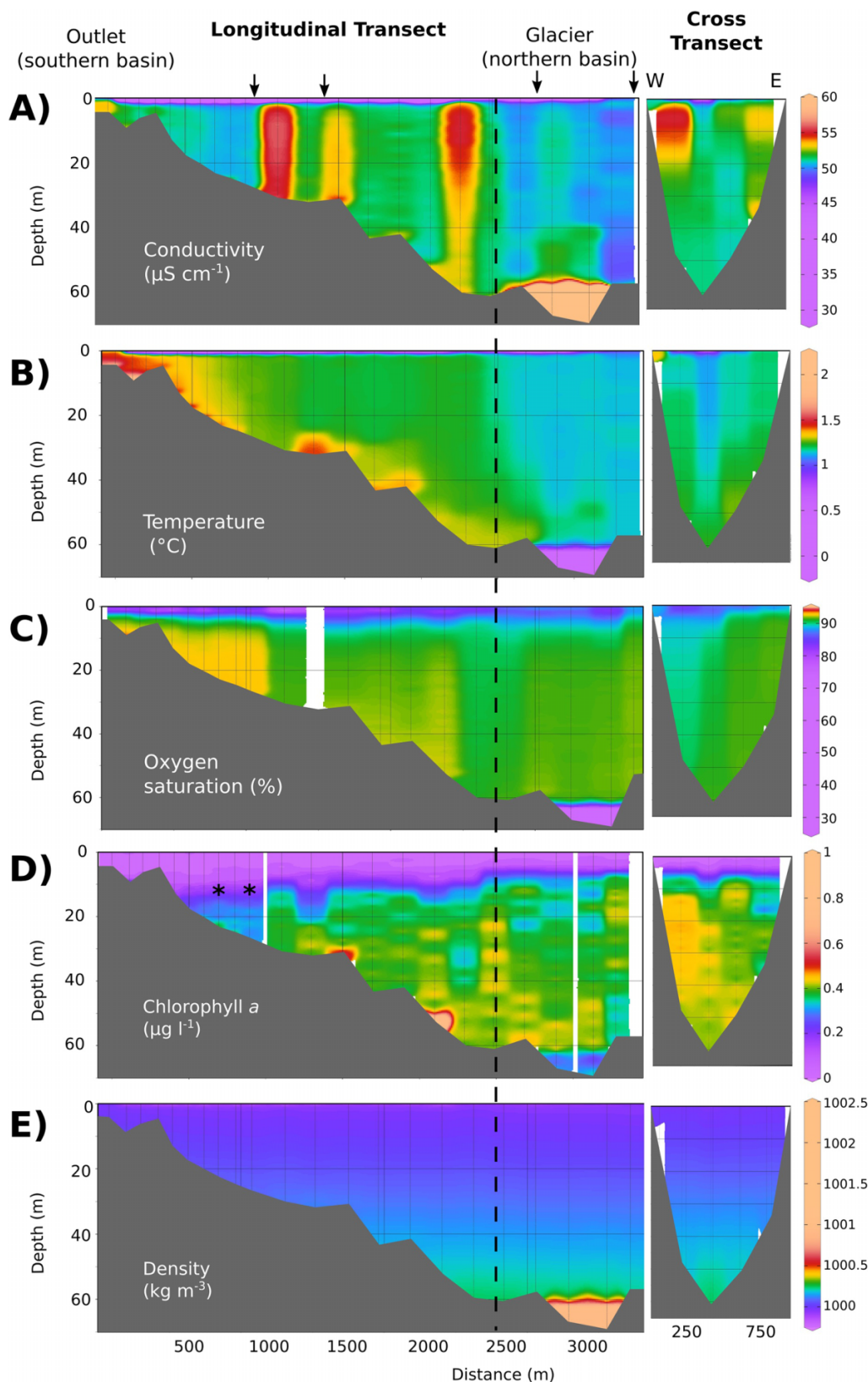
Table 1. Summary of water column properties measured in 2019 with RBRconcerto[3] CTD++ logger.

Measurements	Units	Range	Average
Conductivity	μS cm^{-1}	0–1984	64
Temperature	°C	−0.141 to 2.213	1.19
Chlorophyll a	μg L^{-1}	0–1.77	0.23
Dissolved oxygen	%	26–94	90

the glacier interface and lake outlet ($n = 2$). We filtered 200–4000 mL of water by vacuum filtration onto pre-combusted glass fiber filters (Whatman™), which were stored at −20 °C in the field, and then at −80 °C until freeze-drying for FA analysis. Seston dry weight was measured after freeze-drying. Fatty acid methyl esters (FAMEs) were extracted, methylated, and subjected to gas chromatography–mass spectrometry for identification and quantification using calibration curves as in Grosbois et al. (2022).

Zooplankton were sampled with vertical net tows (53 μm mesh) from three sites in the southern and northern basins, and the glacier interface (Fig. 1C). The net was lowered twice to 20–50 m depending on the site and slowly pulled up to the surface. Samples were preserved with formaldehyde (4%, *v/v*) and counted using Utermöhl chambers and an inverted microscope (Axio Observer A1, Zeiss, Jena, Germany) at 400× magnification.

DNA was extracted directly from Anotop filters using the MasterPure™ Complete DNA & RNA Purification Kit (Lucigen, Middleton, WI, USA) and the backflushing technique described in Mueller et al. (2014). Metagenomic paired-end (2 × 150 bp) libraries were constructed and sequenced on an Illumina NextSeq 550 at the Integrated Microbiome Resource at Dalhousie University, Halifax, Canada, yielding on average 8.6 million (standard deviation (SD) ± 2.1 million) raw read pairs per sample. To filter and trim reads, we used illumina-utils v.2.12 (Eren et al. 2013) and quality thresholds suggested by Minoche et al. (2011) as implemented in the metagenomic workflow in anvi'o v.7.1 (Eren et al. 2021), leaving 93%–94% of read pairs for analyses (Supplementary Table S1).

We extracted 18S ribosomal RNA (18S rRNA) marker genes from these reads using BBMap v.38.93 and the SILVA SSU Ref NR 99 database 138 (Quast et al. 2013) as reference, as implemented in phyloFlash v.3.4 (Gruber-Vodicka et al. 2020), with default settings and a 98% identity threshold for clustering. We used the last-common-ancestor consensus of the top hits to report an approximate taxonomic affiliation and the mapped read counts to generate an overview of community composition across samples. Classifications were manually curated for consistency in reported taxonomic ranks.

Results

Thores Lake ice cover

In 2018, average lake ice thickness from three closely spaced cores in the centre of the northern basin (Fig. 1C) was 1.38 m. In 2019, ice at the same site was 1.01 m, and thickness decreased linearly from 1.42 m near the outflow of the lake to 0.94 m near the glacier terminus (Supplementary Fig. S1). In

the cross transect, the thickest ice was found west of the lake midpoint. All cores included 2–12 cm of white ice, derived from snow and slush. PAR was measured in 2019 at two sites, both in the southern basin, where ice was 1.39 and 1.24 m thick, respectively. An average of 39% of PAR penetrated the ice and entered the water column. The attenuation coefficient in the upper 5 m at the two sites was 0.31 and 0.33 m^{-1}, and decreased below that depth. Estimated euphotic depth (depth of irradiance at 1% of incident values above the ice) was about 12 m (Fig. 2D).

Water column properties

In 2018, water column properties were measured at a single site in the deep northern basin. The effect of ice was detectable with low conductivity and temperature in the upper 80 cm (Fig. 3A). Conductivity was then homogeneous with depth, with a mean of 50 μS cm^{-1}, while temperature below 1 m was stable at 0.8–0.9 °C. Chl a measured by fluorescence indicated ultraoligotrophic conditions, increasing from <0.2 μg L^{-1} at the surface to 0.6 μg L^{-1} at 26 m, and then remaining stable to the bottom of the water column.

In 2019, conductivity was slightly higher in the middle section of the lake, and near the shore in the cross transect (Fig. 2A). Conductivity at the glacier interface was higher than the other surface waters of the lake (250 μS cm^{-1}) and may reflect a higher content of dissolved major ions in the stream inflow near this point. Temperature in the upper water column decreased from 2.3 °C at the surface of the lake outlet to 0.8 °C at the glacier interface, but was 1.1–1.4 °C over most of the lake (Fig. 2B). The density profile showed that most of the lake was characterized by a relatively homogeneous water column (Fig. 2E). Temperature–salinity (specific conductivity) plots confirmed that most of the water column was unstable throughout the lake, with points clustering along a line of equal conductivity (Supplementary Fig. S2). The southern basin had cold surface water of very low conductivity, implying its derivation from melting lake ice, and the distinct T–S properties of the deep water layer in the northern basin indicated that it had little exchange with the rest of the lake (Figs. 2 and 3B).

In 2019, a DO minimum of 77%–81% saturation was located ~1.2 m below the ice, and was more pronounced toward the lake outlet (Fig. 2C). DO saturation below the oxycline was 90%–93%. The chl a profile was similar to 2018, but with lower concentrations in deeper waters (~0.4 μg L^{-1}; Fig. 3B). Patches of higher chl a at the bottom, in some sites as high as 0.7 μg L^{-1}, occurred on a scale of <1 cm, and conductivity values confirmed that it was not an artefact from the probe striking the bottom sediments.

The chl a-containing layer was shallower in 2019 than in 2018, appearing at 14 m depth, ~500 m from the outlet, and shoaling to <6 m near the glacier terminus (Fig. 2D). Chl a fluorescence at the glacier interface (0.24 μg L^{-1}) was high compared with surface waters throughout the lake, which was <0.2 μg L^{-1}, but not as high as in the deep chl a-containing layer of the water column. Chl a fluorescence was higher on the western side of the lake (Fig. 2D).

Fig. 3. Water column properties in Thores Lake from two sites and years. (A) 2018 in northern basin, at site without high-conductivity bottom water. (B) 2019 in northern basin at site with high-conductivity bottom water. Note *x*-axis is the same for temperature and chlorophyll *a* and different for conductivity and dissolved oxygen. Chlorophyll *a* data have been treated with kernel smoothing.
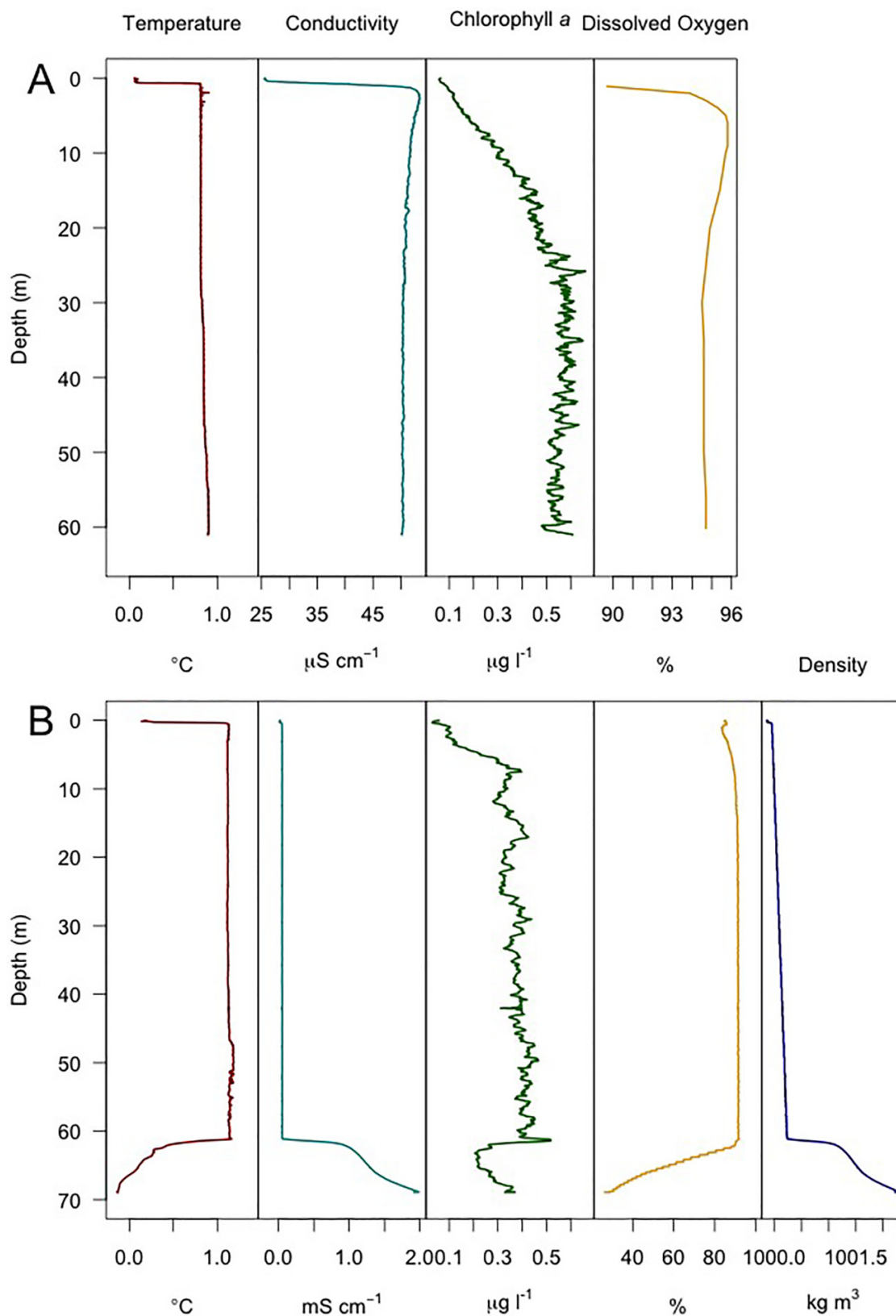
Table 2. Physico-chemical properties of Thores Lake in the Canadian High Arctic in July 2019.

Sample	Temperature (°C)	Conductivity (μS cm^{-1})	Total phosphorus (μg L^{-1})	Total nitrogen (μg L^{-1})	NO$_2$ + NO$_3$ nitrogen (μg L^{-1})	Dissolved organic carbon (mg L^{-1})	Seston dry weight (mg L^{-1})
Water column							
5 m	1.2	51	6.2	75	55	0.03	1.8
15 m	1.2	50	5.6	61	55	0.00	1.8
Surface							
Glacier interface	0.79	250	85	59	47	0.04	69
Lake outlet	2.3	57	6.7	103	51	0.00	1.3

Note: Water column measurements are from a site in the southern basin of the lake ("N" in Fig. 1C). Surface samples are from <0.5 m depth.

Fig. 4. Chlorophyll *a* concentration and mass ratios of accessory pigments in the lake outlet surface, lake ice, water column, and glacier interface surface water of Thores Lake in 2018.
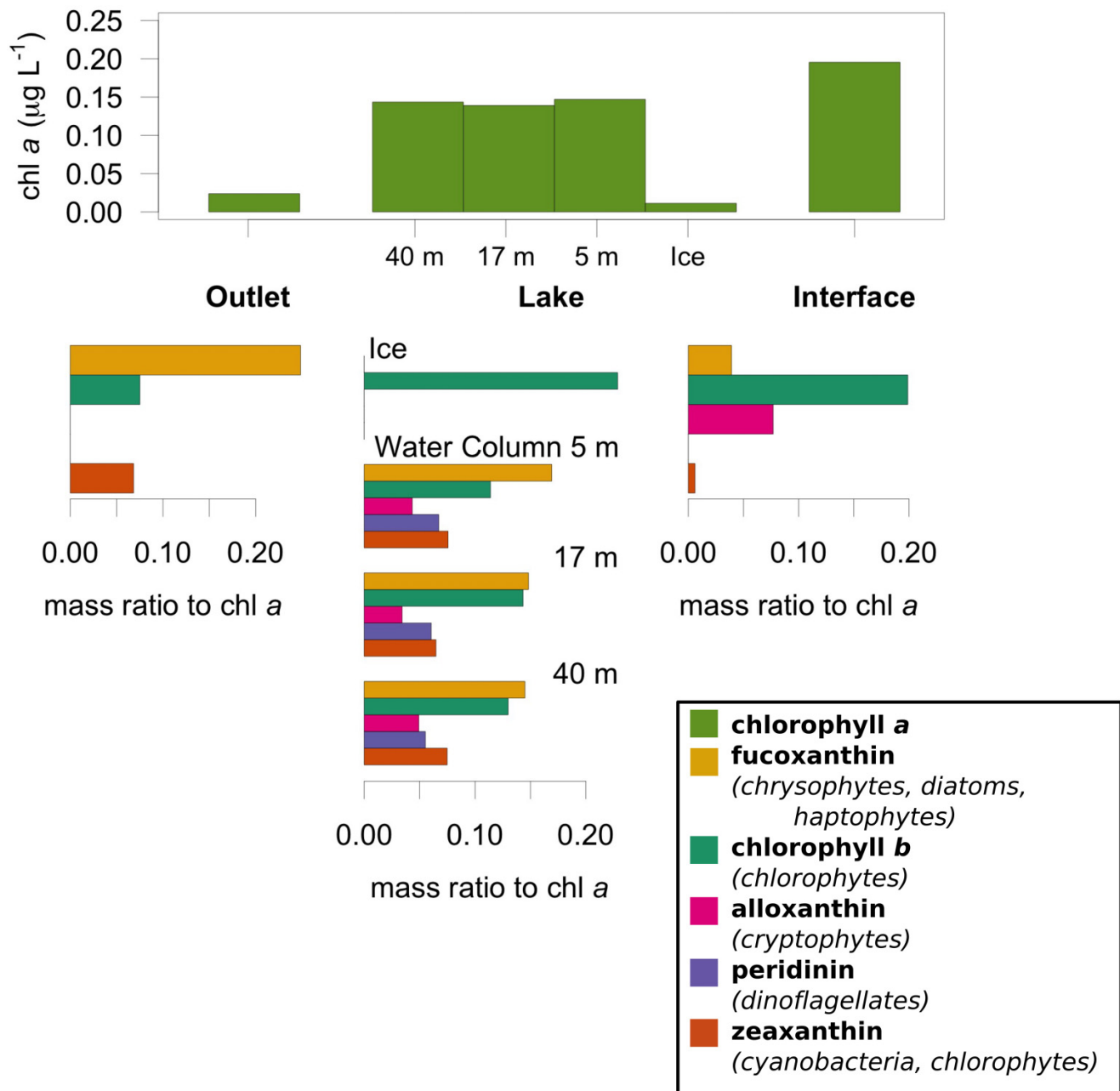
Fig. 5. Major taxonomic groups in eukaryote 18S rRNA sequences and taxonomic composition of the metazoan taxa.
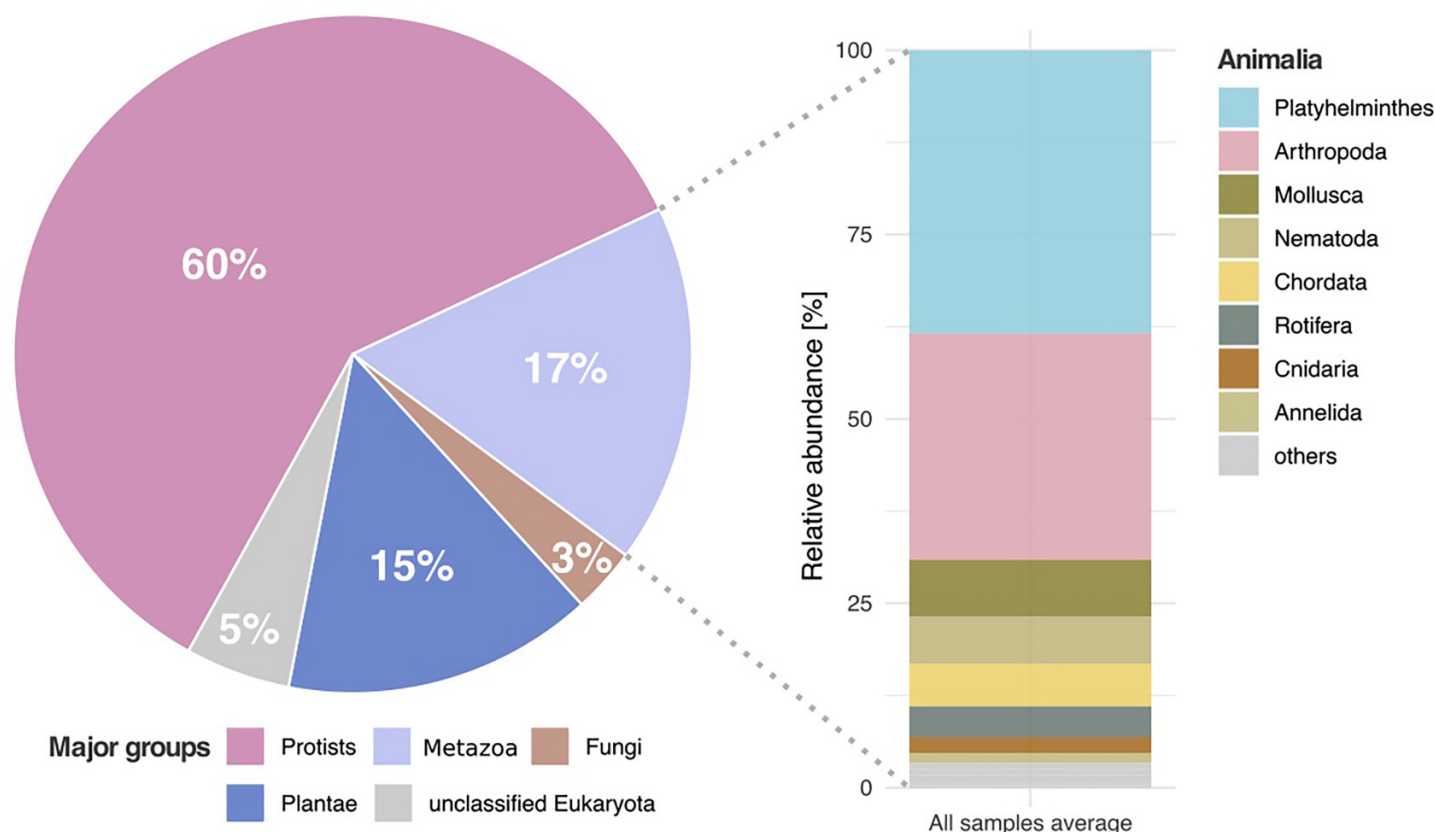
We detected a depression in the deepest part of the lake, at least 200 m wide in one dimension and 7–9 m deep, with contrasting properties to the rest of the water column (Figs. 2 and 3B). Water in this depression had a minimum temperature of -0.14 °C, with a specific conductivity of 1900 μS cm^{-1}, DO concentration of 26%, and chl a concentration <0.3 μg L^{-1}. The volume of water in this depression was approximately 0.5 km^3.

TP, measured in 2019, was an order of magnitude higher in surface water at the glacier interface than in either the water column of the southern basin or the outlet surface water (Table 2). TN was somewhat higher in outlet surface water; however, NO$_3$ was similar to samples in the lake and glacier interface. It is unlikely that the higher N in the outlet was organic nitrogen, since DOC in this sample was so low, leaving the possibility that it might come from soil erosion. Turbidity, measured as seston weight per volume, was similar in the lake water column and outlet, but almost 40 times higher at the glacier interface. DOC in all samples was at or below the limit of detection (0.03 mg L^{-1}).
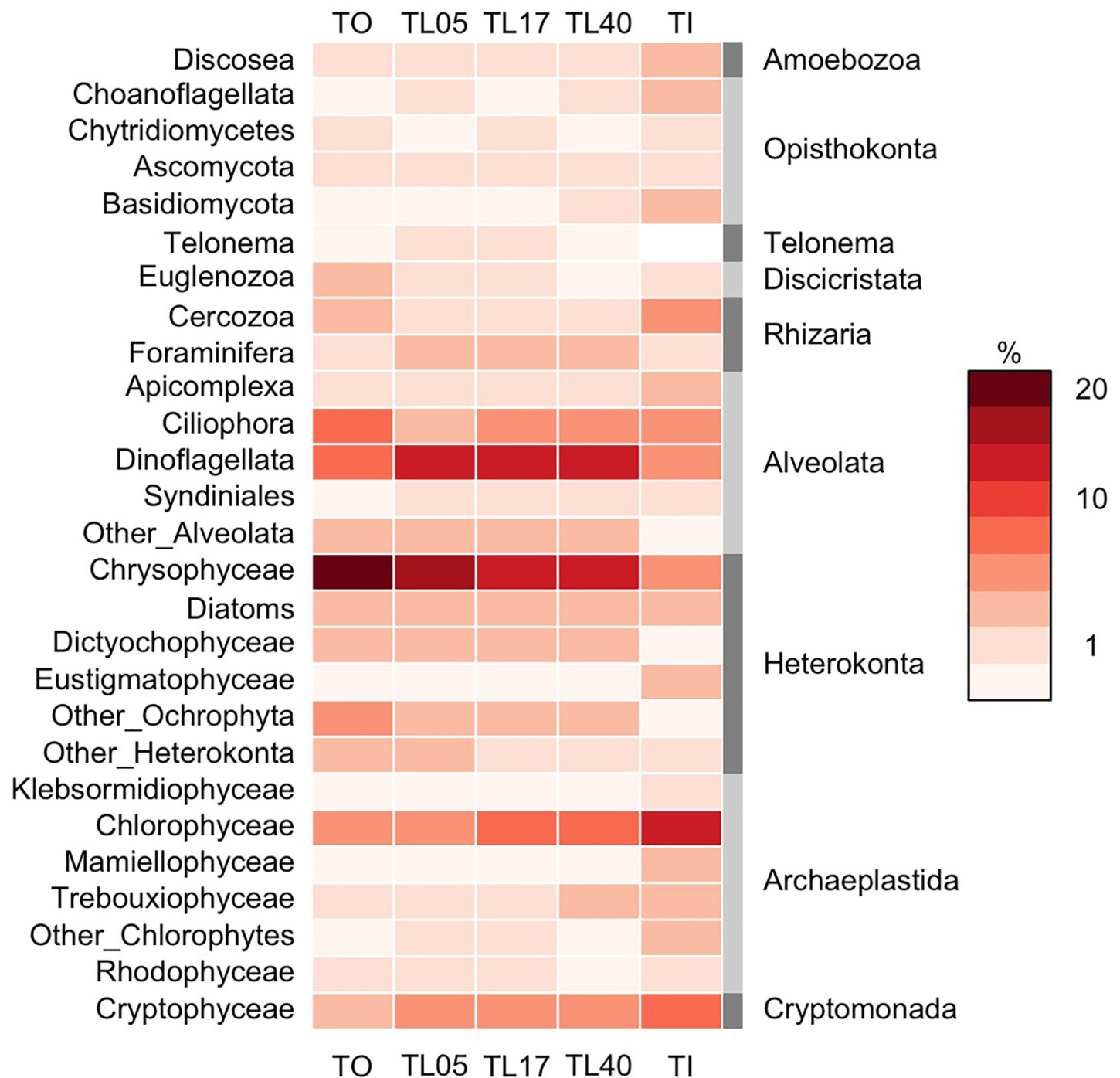
Pigments

Concentrations of chl a measured by HPLC in 2018 in the northern basin (Fig. 4) were lower than those measured using fluorescence (Fig. 3A), and did not vary with water column depth. Chl a was somewhat higher at the glacier interface, and much lower in the ice core and out-

let surface water (Fig. 4). We examined accessory pigment ratios as markers of taxonomic composition following Wright and Jeffrey (2006), including zeaxanthin (cyanobacteria and chlorophytes), peridinin (dinoflagellates), alloxanthin (cryptophytes), chlorophyll b (chl b; chlorophytes), and fucoxanthin (found in chrysophytes, diatoms, and haptophytes). Small quantities of the cryptophyte pigment crocoxanthin (0.003–0.005 ratio to chl a) also co-occurred with alloxanthin wherever the latter was present. Pigment composition was similar throughout the water column, but differed between the lake outlet, ice core, and glacier interface. Lutein/chl b ratios were >0.3 in all samples, indicating that the green algae detected were chlorophytes and not prasinophytes.

Metagenomic analyses

Protists accounted for the majority of 18S rRNA sequences in our data (Fig. 5), followed by metazoans. Metazoan sequences belonged to eight phyla: Platyhelminthes, Arthropoda, Mollusca, Nematoda, Chordata, Rotifera, Cnidaria, and Annelida (Fig. 5). This taxonomic diversity is broader than that suggested by our zooplankton sampling, and likely includes DNA from two additional sources: potential benthic organisms (which were not targeted by our sampling) and terrestrial runoff, including parasites in animal feces. Sequences of land plants included dicotyledon angiosperms and conifers, none of which belonged to local species (data

Fig. 6. Protist and fungi taxonomic groups as percentage of total hits to 18S rRNA genes in Thores Lake in July 2018. TO, outlet surface; TL, lake water column at 5, 17, and 40 m depth; and TI, glacier interface surface. Values represent pooled triplicates ($n = 3$). Colour scale is square-root transformed. Metazoa and terrestrial plants are not shown (see Fig. 5).

not shown). These may represent wind-blown pollen transport. Sequences of fungi included putative terrestrial and aquatic taxa.

In general, the metagenomic identification of photosynthetic protists was consistent with the pigment data. Compared with the lake outlet and the deeper water column samples, surface water at the glacier interface had a much higher proportion of green algal taxa (phylum Chlorophyta)

particularly in the class Chlorophyceae, while the relative abundance of Dinophyceae and Chrysophyceae was lower (Figs. 6 and 7). Dinoflagellates were dominated by photosynthetic genera such as *Biecheleria*, *Polarella*, and *Symbiodinium* (Fig. 7). Chrysophyceae sequences had a higher relative abundance in the lake, and particularly the lake outlet, where they may be responsible for the higher ratio of fucoxanthin pigment. Other eukaryotic taxa, including diatoms and cili-

Fig. 7. Phytoplankton genera as percentage of total hits to 18S rRNA genes in Thores Lake in 2018. TO, outlet surface; TL, lake water column at 5, 17, and 40 m depth; and TI, surface water at glacier interface. Values represent pooled triplicates ($n = 3$). Tree at top of figure shows clustering of samples by Bray–Curtis dissimilarity. Colour scale is square-root transformed. Note that dinoflagellate genera *Gymnodinium* and *Pfiesteria* (labelled H) comprise some or all heterotrophic species, while other dinoflagellate genera are phototrophic.
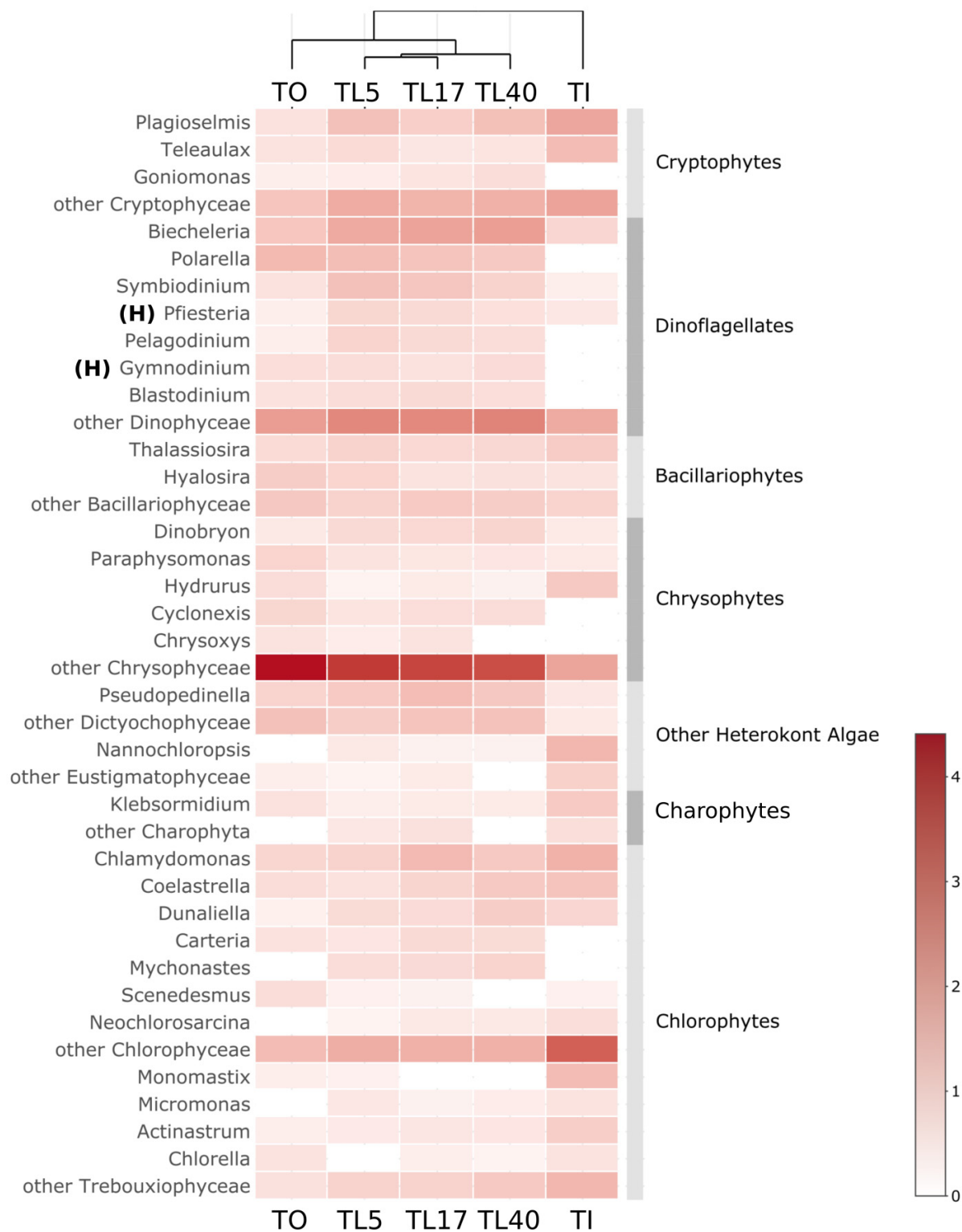
Fig. 8. Fatty acid methyl esters (FAMEs) in seston samples from Thores Lake in surface water at the glacier interface, in the lake water column, and lake outlet surface: (A) total FAME and (B) omega-3 fatty acid concentration ($n = 2$; duplicate water column samples are from 5 and 15 m).
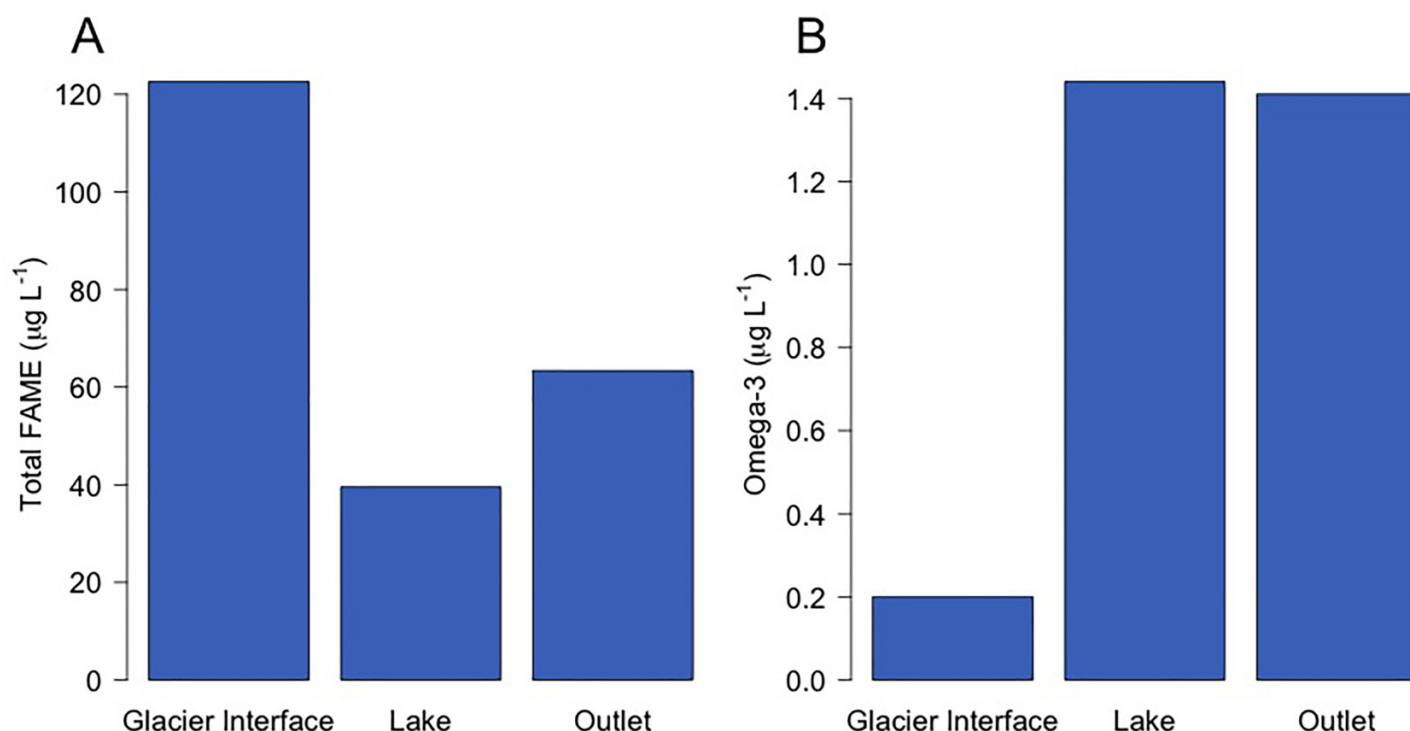
Fig. 9. Zooplankton taxa in the upper 50 m of Thores Lake, ordered by abundance (ind. m^{-3}). Error bars show mean $\pm$ standard error ($n = 3$). Note log scale on *y*-axis. Taxa that had highest abundance at the glacier interface are indicated with an asterisk.
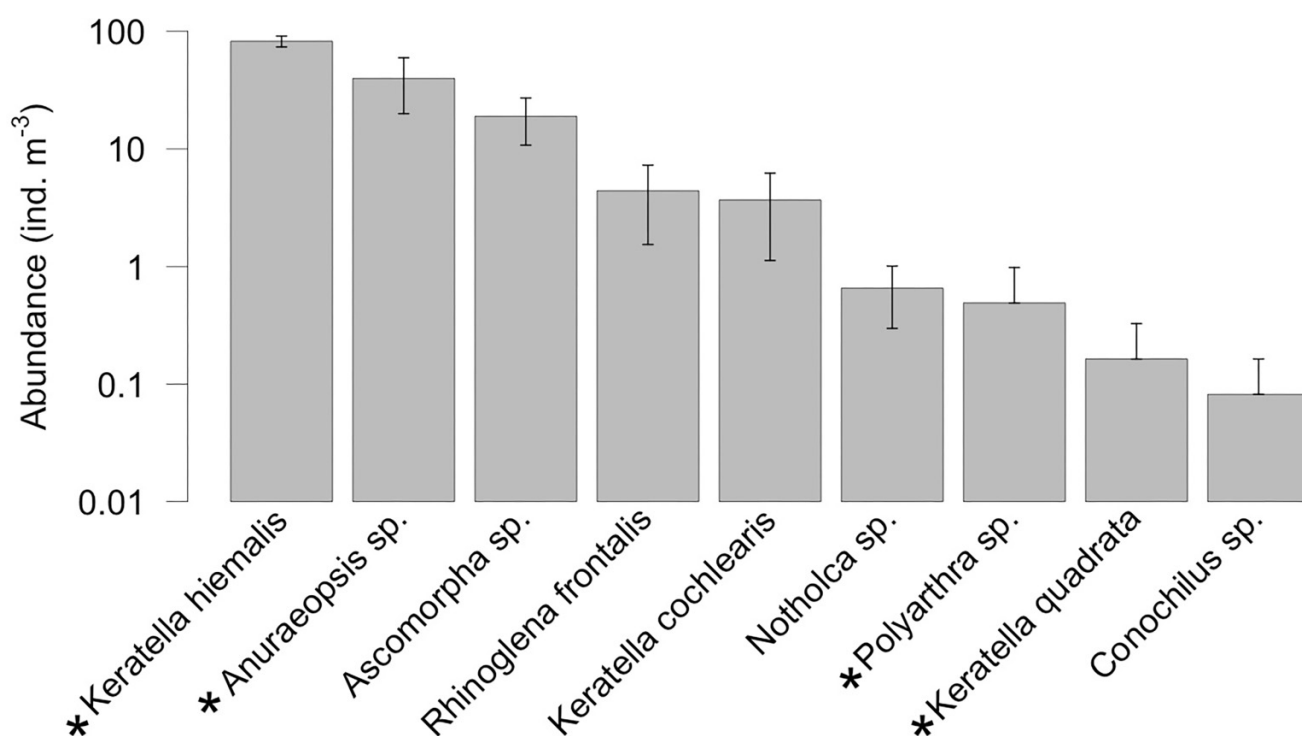
ates, were found at uniform relative abundance in all environments in the lake.

Fatty acids

FA content was measured from the same samples collected for turbidity, and varied by environment (Fig. 8). Turbid surface waters at the glacier interface had high total FAME, comprising >90% of saturated FAs. Omega-3 FA in this environment contributed <1% of total FAME. Water in the centre of the lake and at the lake outlet had lower FAME content, but higher prevalence of omega-3 FA, comprising 3.6% and 2.2% of FA, respectively.

Zooplankton

We found only rotifers in the zooplankton samples, and no copepods or cladocerans (Fig. 9). While species richness was similar in the two lake samples and glacier interface, community composition differed. Two taxa, *Polyarthra* sp. and *Keratella quadrata*, were found only at the glacier interface, and two of the taxa that were present in all samples, *Anuraeopsis* sp. and *K. hiemalis*, had their highest abundance (79 and 95 ind. m^{-3}, respectively) at the interface (Fig. 9). *Keratella hiemalis* was the most abundant taxon overall. *Conochilus* sp. is colonial, and was the only taxon that showed signs of reproduction, with 4.7% of individuals carrying eggs. It was found only in the northern basin of the lake.

Conclusions

While a number of lakes in northern Ellesmere Island have been well described with respect to their evolution and responses to climate change (Van Hove et al. 2006), to our knowledge Thores Lake is the first data set to characterize a proglacial lake in this region, and may serve as a model for other high-latitude proglacial lakes. Our data show typical features of proglacial lakes, including limited zooplankton diversity (Sommaruga 2015) and horizontal gradients of temperature and nutrients (Burpee et al. 2018). The observations also highlight the importance of surface waters at the glacier interface as a unique environment characterized by higher chl *a* (Fig. 4 and Table 2), lower omega-3 FA (Fig. 8), and a distinctive protist community (Fig. 6). Primary production in Thores Lake is very low (ultraoligotrophic), although high chl *a* fluorescence at two sites at the bottom of the water column (Fig. 2D) may indicate a more productive deep-water phytoplankton. Benthic microbial mats are also likely to contribute to primary production in Thores Lake, as in many oligotrophic polar lakes elsewhere (e.g., Lionard et al. 2012; Mohit et al. 2017; Greco et al. 2020).

Future sampling of Thores Lake will aim to measure how it changes in response to climate change from the baseline established by the present data set. Air temperatures in this region have been highly variable over the past 13 years, with warm years associated with loss of multi-year ice cover in several coastal lakes (Mueller et al. 2009; Bégin et al. 2021a). The cooling effect of the glacier adjacent to Thores Lake may ex-

plain why it retained at least partial ice cover even in 2016, the warmest year on record (Supplementary Video S1). Loss of summer ice cover may increase chl *a* biomass through increased PAR and nutrient entrainment by mixing (Bégin et al. 2021a). While wind-driven mixing would increase during the ice-free period, the steep density gradient of the bottom water (Fig. 2E) might be strong enough to resist entrainment. If the current stability of Thores Glacier continues, this in combination with the sheltered, inland position of Thores Lake may protect it from marked changes in ice cover and mixing, and preserve it as an ice-capped proglacial Arctic ecosystem.

Acknowledgements

Article information

History dates

Notes

This data paper is a contribution to the T-MOSAiC special issue "Terrestrial Geosystems, Ecosystems and Human Systems in the Fast-Changing Arctic".

Copyright

Data availability

Physico-chemical profiles have been deposited in the archive Nordicana D under accession number D82 (Culley et al. 2022; http://doi.org/10.5885/45669CE-3078BA69AC9944CA).

Pigments are under accession number D26 (NEIGE 2022; http://doi.org/10.5885/45436CE-0E0A89CB98C148F4). Nutrients, DOC, zooplankton, and FAs are under accession number D105 (Girard et al. 2022; http://doi.org/10.5885/45801CE-647F4C260BD64AEC). Raw sequences are archived in the NCBI Short Read Archive at PRJNA832578.

Author information

Author ORCIDs

Alexander I. Culley https://orcid.org/0000-0001-6639-9112
William Kochtitzky https://orcid.org/0000-0001-9487-1509
Josephine Z. Rapp https://orcid.org/0000-0001-5812-6405
Warwick F. Vincent https://orcid.org/0000-0001-9055-1938
Catherine Girard https://orcid.org/0000-0002-3899-0180

Author notes

Present address for William Kochtitzky is School of Marine and Environmental Programs, University of New England, Biddeford, ME, USA.

Present address for Alexander Culley is Pacific Biosciences Research Center, University of Hawai'i at Mānoa, Honolulu, HI, USA.

Luke Copland and Warwick Vincent served as Associate Editors at the time of manuscript review and acceptance and did not handle peer review and editorial decisions regarding this manuscript.

Author contributions

Conceptualization: AIC, LC, WFV, CG
Data curation: MT, JZR, CG
Investigation: WK, PI, MR, CG
Project administration: AIC, LC, WFV
Visualization: MT, WK, JZR, MR
Writing – original draft: MT, WK, JZR, MR
Writing – review & editing: AIC, MT, WK, JZR, MR, MK, LC, WFV, CG

Competing interests

The authors declare there are no competing interests.

Supplementary material

Supplementary data are available with the article at https://doi.org/10.1139/as-2022-0023.

References

Bégin, P.N., Tanabe, Y., Kumagai, M., Culley, A.I., Paquette, M., Sarrazin, D., et al. 2021a. Extreme warming and regime shift toward amplified variability in a far northern lake. Limnol. Oceanogr. **66**: S17–S29. doi:10.1002/lno.11546.

Bégin, P.N., Tanabe, Y., Rautio, M., Wauthy, M., Laurion, I., Uchida, M., et al. 2021b. Water column gradients beneath the summer ice of a High Arctic freshwater lake as indicators of sensitivity to climate change. Sci. Rep. **11**: 2868. doi:10.1038/s41598-021-82234-z.

Burpee, B.T., Anderson, D., and Saros, J.E. 2018. Assessing ecological effects of glacial meltwater on lakes fed by the Greenland ice sheet: the role of nutrient subsidies and turbidity. Arctic Antarctic Alpine Res. **50**: S100019. doi:10.1080/15230430.2017.1420953.

Culley, A.I., Girard, C., and Vincent, W.F. 2022. Physico-chemical profiles in proglacial Thores Lake, Ellesmere Island, Nunavut, v. 1.1. Nordicana, **D82**. doi:10.5885/45669CE-3078BA69AC9944CA.

Cuthbert, I.D., and del Giorgio, P. 1992. Toward a standard method of measuring color in freshwater. Limnol. Oceanogr. **37**(6): 1319–1326. doi:10.4319/lo.1992.37.6.1319.

Dranga, S.A., Hayles, S., and Gajewski, K. 2018. Synthesis of limnological data from lakes and ponds across Arctic and Boreal Canada. Arctic Sci. **4**(2): 167–185. doi:10.1139/as-2017-0039.

Eren, A.M., Vineis, J.H., Morrison, H.G., and Sogin, M.L. 2013. A filtering method to generate high quality short reads using Illumina paired-end technology. PloS ONE, **8**(6): 0066643. doi:10.1371/journal.pone.0066643.

Eren, A.M., Kiefl, E., Shaiber, A., Veseli, I., Miller, S.E., Schechter, M.S., et al. 2021. Community-led, integrated, reproducible multi-omics with anvi'o. Nat. Microbiol. **6**: 2–6. doi:10.1038/s41564-020-00834-3.

Filazzola, A., Mahdiyan, O., Shuvo, A., Ewins, C., Moslenko, L., Sadid, T., et al. 2020. A database of chlorophyll and water chemistry in freshwater lakes. Sci. Data, **7**: 310. doi:10.1038/s41597-020-00648-2. PMID: 32963248.

Girard, C., Rautio, M., Culley, A.I., and Vincent, W.F. 2022. Plankton and water chemistry data from proglacial Thores Lake. v. 1.0. Nordicana, **D105**. doi:10.5885/45801CE-647F4C260BD64AEC.

Greco, C., Andersen, D.T., Hawes, I., Bowles, A., Yallop, M.L., Barker, G., et al. 2020. Microbial diversity of pinnacle and conical microbial mats in the perennially ice-covered Lake Untersee, East Antarctica. Front. Microbiol. **11**: 3173. doi:10.3389/fmicb.2020.607251.

Grosbois, G., Power, M., Evans, M., Koehler, G., and Rautio, M. 2022. Content, composition, and transfer of polyunsaturated fatty acids in an Arctic lake food web. Ecosphere, **13**(1): e03881. doi:10.1002/ecs2.3881.

Gruber-Vodicka, H.R., Seah, B.K.B., and Pruesse, E. 2020. phyloFlash: rapid small-subunit rRNA profiling and targeted assembly from metagenomes. mSystems, **5**(5): e00920–e00920. doi:10.1128/mSystems.00920-20.

Kochtitzky, W., Copland, L., Wohlleben, T., Iqaluk, P., Girard, C., Vincent, W.F., et al. 2022. Slow change since the little ice age at a far northern glacier with the potential for system reorganization: Thores Glacier, Northern Ellesmere Island, Canada. Arctic Sci. In press. doi:10.1139/as-2022-0012.

Lionard, M., Péquin, B., Lovejoy, C., and Vincent, W.F. 2012. Benthic cyanobacterial mats in the High Arctic: multi-layer structure and fluorescence responses to osmotic stress. Front. Microbiol. **3**: 140. doi:10.3389/fmicb.2012.00140. PMID: 22557996.

Millero, F, Chen, C., Bradshaw, A., and Schleicher, K. 1980. A new high pressure equation of state for seawater. Deep Sea Res. A. Oceanogr. Res. **27**: 255–264. doi:10.1016/0198-0149(80)90016-3.

Minoche, A.E., Dohm, J.C., and Himmelbauer, H. 2011. Evaluation of genomic high-throughput sequencing data generated on Illumina HiSeq and Genome Analyzer Systems. Genome Biol. **12**(11): R112. doi:10.1186/gb-2011-12-11-r112. PMID: 22067484.

Mohit, V., Culley, A., Lovejoy, C., Bouchard, F., and Vincent, W.F. 2017. Hidden biofilms in a far northern lake and implications for the changing Arctic. NPJ Biofilms Microbiomes, **3**: 17. doi:10.1038/s41522-017-0024-3.

Mueller, D.R., Van Hove, P., Antoniades, D., Jeffries, M.O., and Vincent, W.F. 2009. High Arctic lakes as sentinel ecosystems: cascading regime shifts in climate, ice cover, and mixing. Limnol. Oceanogr. **54**(6 part 2): 2371–2385. doi:10.4319/lo.2009.54.6_part_2.2371.

Mueller, J.A., Culley, A.I., and Steward, G.F. 2014. Variables influencing extraction of nucleic acids from microbial plankton (viruses, bacteria, and protists) collected on nanoporous aluminum oxide filters. Appl. Environ. Microbiol. **80**(13): 3930–3942. doi:10.1128/AEM.00245-14. PMID: 24747903.

NEIGE. 2017. Water column physico-chemical profiles of lakes and fiords along the northern coastline of Ellesmere Island, v. 1.1 (1954–2016). Nordicana, **D27**. doi:10.5885/45445CE-7B8194DB81754841.

NEIGE. 2022. Phytoplankton pigments of lakes and fiords of northern Ellesmere Island, Nunavut, Canada, v. 1.1. Nordicana, **D26**. doi:10.5885/45436CE-0E0A89CB98C148F4.

Patton, C.J., and Kryskalla, J.R. 2003. Methods of analysis by the U.S. Geological Survey National Water Quality Laboratory—evaluation of al-

kaline persulfate digestion as an alternative to Kjeldahl digestion for determination of total and dissolved nitrogen and phosphorus. Vol. 3. US Department of the Interior, US Geological Survey, Reston, VA, U.S.A. p. 4174.

Planet Team. 2017. Planet application program interface. In Space for life on Earth. Planet Team, San Francisco, CA.

Quast, C., Pruesse, E., Yilmaz, P., Gerken, J., Schweer, T., Yarza, P., et al. 2013. The SILVA ribosomal RNA gene database project: improved data processing and web-based tools. Nucleic Acids Res. **41**: D590–D596. doi:10.1093/nar/gks1219. PMID: 23193283.

Schlitzer, R. 2015. Ocean Data View. Version 4.7.4. Available from http://odv.awi.de.

Sommaruga, R. 2015. When glaciers and ice sheets melt: consequenes for planktonic organisms. J. Plankton Res. **37**(3): 509–518. doi:10.1093/plankt/fbv027. PMID: 26869738.

Stolpmann, L., Coch, C., Morgenstern, A., Boike, J., Fritz, M., Herzschuh, U., et al. 2021. First pan-Arctic assessment of dissolved organic carbon in lakes of the permafrost region. Biogeosciences, **18**: 3917–3936. doi:10.5194/bg-18-3917-2021.

Sui, Y., Feng, M., Wang, C., and Li, X. 2022. A high-resolution inland surface water body dataset for the Tundra and Boreal forests of North America. Earth Syst. Sci. Data, **14**: 3349–3363. doi:10.5194/essd-14-3349-2022.

Thaler, M., Vincent, W.F., Lionard, M., Hamilton, A.K., and Lovejoy, C. 2017. Microbial community structure and interannual change in the last epishelf lake ecosystem in the North Polar region. Front. Mar. Sci. **3**: 275. doi:10.3389/fmars.2016.00275.

Van Hove, P., Belzile, C., Gibson, J.A.E., and Vincent, W.F. 2006. Coupled landscape–lake evolution in High Arctic Canada. Can. J. Earth Sci. **43**(5): 533–546. doi:10.1139/E06-003.

Vincent, W.F., and Mueller, D. 2020. Witnessing ice habitat collapse in the Arctic. Science, **370**(6520): 1031–1032. doi:10.1126/science.abe4491. PMID: 33243873.

Vincent, W.F., Canário, J., and Boike, J. 2019. Understanding the terrestrial effects of Arctic Sea ice decline. Eos Earth Space News, **100**. doi:10.1029/2019EO128471.

Vincent, W.F., Fortier, D., Lévesque, E., Boulanger-Lapointe, N., Tremblay, B., Sarrazin, D., et al. 2011. Extreme ecosystems and geosystems in the Canadian High Arctic: Ward Hunt Island and vicinity. Ecoscience, **18**(3): 236–261. doi:10.2980/18-3-3448.

Wauthy, M., Rautio, M., Christoffersen, K.S., Forsström, L., Laurion, I., Mariash, H., et al. 2017. Dissolved organic carbon and related environmental data from ponds and lakes in the circumpolar North, v. 1.0 (2002–2016). Nordicana, **D31**. doi:10.5885/45520CE-0A48ADE0E2194290.

Wetzel, R.G., and Likens, G.E. 2000. Limnological analyses. Springer Press.

White, A., and Copland, L. 2019. Loss of floating glacier tongues from the Yelverton Bay region, Ellesmere Island, Canada. J. Glaciol. **65**(251): 376–394. doi:10.1017/jog.2019.15.

Wright, S.W., and Jeffrey, S.W. 2006. Pigment markers for phytoplankton production, *In* Marine organic matter: biomarkers, isotopes and DNA. *Edited by* J.K. Volkman. Springer, Berlin, Germany. pp. 71–104.